BIOCHEMISTRY
including biophysical chemistry & molecular biology

ARTICLE

pubs.acs.org/biochemistry

Energetics for Oxidation of a Bound Manganese Cofactor in Modified Bacterial Reaction Centers

L. Kálmán,[‡] J. C. Williams, and J. P. Allen*

Department of Chemistry and Biochemistry, Arizona State University, Tempe, Arizona 85287-1604, United States

Supporting Information

ABSTRACT: The energetics of a Mn cofactor bound to modified reaction centers were determined, including the oxidation/reduction midpoint potential and free energy differences for electron transfer. To determine these properties, a series of mutants of *Rhodobacter sphaeroides* were designed that have a metal-ion binding site that binds Mn^{2+} with a dissociation constant of 1 μM at pH 9.0 (Thielges et al. (2005) *Biochemistry 44*, 7389−7394). In addition to the Mn binding site, each mutant had changes near the bacteriochlorophyll dimer, P, that resulted in altered P/P^+ oxidation/reduction midpoint potentials, which ranged from 480 mV to above 800 mV compared to 505 mV for wild type. The bound Mn^{2+} is redox active and after light excitation can rapidly reduce the oxidized primary electron donor, P^+. The extent of P^+ reduction was found to systematically range from a full reduction in the mutants with high P/P^+ midpoint potentials to no reduction in the mutant with a potential comparable to wild type. This dependence of the extent of Mn^{2+} oxidation on the P/P^+ midpoint potential can be understood using an equilibrium model and the Nernst equation, yielding a Mn^{2+}/Mn^{3+} oxidation/reduction midpoint potential of 625 mV at pH 9. In the presence of bicarbonate, the Mn^{2+}/Mn^{3+} potential was found to be 90 mV lower with a value of 535 mV suggesting that the bicarbonate serves as a ligand to the bound Mn. Measurement of the electron transfer rates yielded rate constants for Mn^{2+} oxidation ranging from 30 to 120 s^{-1} as the P/P^+ midpoint potentials increased from 670 mV to approximately 805 mV in the absence of bicarbonate. In the presence of bicarbonate, the rates increased for each mutant with values ranging from 65 to 165 s^{-1}, reflecting an increase in the free energy difference due to the lower Mn^{2+}/Mn^{3+} midpoint potential. This dependence of the rate constant on the P/P^+ midpoint potential can be understood using a Marcus relationship that yielded limits of at least 150 s^{-1} and 290 meV for the maximal rate constant and reorganization energy, respectively. The implications of these results are discussed in terms of the energetics of proteins with redox active Mn cofactors, in particular, the Mn_4Ca cofactor of photosystem II.

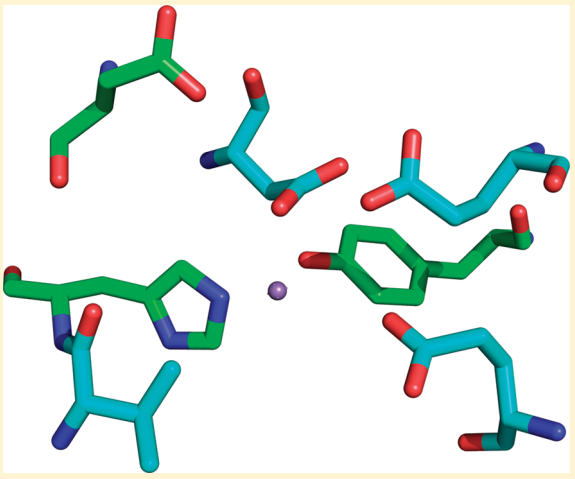

Oxidation and reduction reactions involving metal-ion cofactors such as manganese, iron, and copper play important roles in the function of many proteins. A critical parameter for the ability of a metal-ion cofactor to participate in such reactions is the oxidation/reduction midpoint potential of the metal. Because the midpoint potentials of metal cofactors in proteins can vary widely depending on factors such as the ligands and the pH, they can be tailored to fit a range of reactions. However, direct measurements of this key parameter for manganese in proteins have proven to be difficult; for example, determination of the midpoint potential of the metal cofactor of superoxide dismutase has been limited due to factors such as poor equilibration of the metal center with the electrodes. Measurements have been possible only with the use of proper mediators involving equilibration times that can be up to several hours.[1] For metals with oxidation potentials above that of water, the potentials cannot be measured directly. For example, the site of water oxidation in oxygenic photosynthesis takes place at the Mn_4Ca cluster that is located in photosystem II. In this case, the potentials of the Mn_4Ca cluster have never been directly measured and are only inferred based upon models of the electron transfer rates.[2−4]

In anoxygenic photosynthesis, purple bacteria contain a pigment−protein complex termed the reaction center that is the site of the primary photochemistry, namely, the conversion of light energy into a charge-separated state.[5] Upon excitation, the primary electron donor, P, which is a bacteriochlorophyll dimer, transfers an electron through a series of acceptors to the primary quinone, Q_A, followed by transfer to the secondary quinone. In wild type, the oxidized donor, P^+, is reduced by an exogenous cytochrome c_2, after which it can be excited again leading to the transfer of a second electron to the secondary quinone in a process that is coupled to the uptake of two protons.

Received: November 1, 2010
Revised: March 3, 2011
Published: March 04, 2011

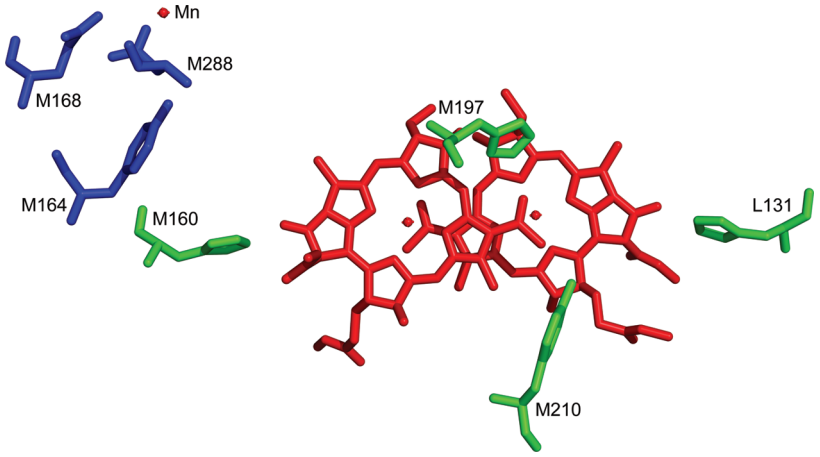

Figure 1. Three-dimensional structure of M2 mutant. Shown are the amino acid residues that have been altered to introduce a Mn binding site, Tyr M164, Glu M168, and Asp M288 (blue), and residues that result in an increase the P/P^+ midpoint potential compared to wild type, His L131, His M160, His M197, and Tyr M210 (green). Also shown are the bacteriochlorophyll dimer P and bound Mn (red). All of the mutants characterized have the same Mn binding site but different mutations near P resulting in a range of P/P^+ midpoint potentials for the mutants. Data are from PDB file 1Z9J.[9]

The secondary quinone carries the electrons and protons to the cytochrome bc_1 complex in a cycle that generates the proton gradients needed for the creation of energy-rich compounds. Photosystem II follows a similar electron transfer pathway from the primary electron donor to the quinones; however, the Mn_4Ca cluster serves as the secondary electron donor rather than an exogenous secondary electron donor. Despite this key functional difference, the core of the reaction center has a strong structural homology to the core of photosystem II and can be manipulated such that it gains a Mn cofactor serving as a secondary donor.[6] To achieve this function, reaction centers from *Rhodobacter sphaeroides* were altered such that they became highly oxidizing by introducing histidines that can serve as proton donors to the conjugated system of P.[7,8] Specifically, three amino acid residues, Leu L131, Leu M160, and Phe M197, were altered to histidine, with each change increasing the oxidation/reduction midpoint potential of P, $E_m(P/P^+)$, by 60−120 mV while replacing Tyr M210 with Trp increases the potential by 44 mV[7−12] (Figure 1). The combination of the four substitutions increases $E_m(P/P^+)$ by approximately 300 mV compared to a value of 500 mV for wild type.

The highly oxidizing reaction centers were modified to bind a single Mn^{2+} at a site corresponding to the Mn_4Ca cluster in photosystem II.[9,10] In this mutant, identified as the M2 mutant, the bound Mn^{2+} is redox active and can rapidly reduce P^+ in a first-order reaction. To probe the energetics of the Mn cofactor, a series of reaction center mutants were designed with each containing the Mn binding site found in the M2 mutant defined by the following three substitutions: Arg M164 to Tyr, Met M168 to Glu, and Gly M288 to Asp (Figure 1). With these changes, the mutants should be capable of binding Mn at the site where the metal-ion can serve as an efficient electron donor. The extent of metal oxidation depends upon the relative oxidation/reduction potentials of the bound Mn and P. In order to fully oxidize the bound Mn^{2+}, the oxidation/reduction midpoint potential of P, $E_m(P/P^+)$, must be well above $E_m(Mn^{2+}/Mn^{3+})$. If $E_m(P/P^+)$ is small compared to $E_m(Mn^{2+}/Mn^{3+})$, then no oxidation of the bound Mn^{2+} will be observed. Thus, the extent of Mn^{2+} oxidation provides an opportunity to determine the $E_m(Mn^{2+}/Mn^{3+})$ potential by monitoring the oxidation state of P for mutants with different $E_m(P/P^+)$ potentials. Therefore, in addition to changes designed to bind Mn, the mutants have various combinations of the amino acid substitutions near P that increase $E_m(P/P^+)$ compared to wild type: Leu L131 to His, Leu M160 to His, Phe M197 to His, and Tyr M210 to Trp (Figure 1). Since the effect of these mutations is additive, the use of combinations of these four alterations near P should result in a wide range of $E_m(P/P^+)$ potentials for the mutants.

Bicarbonate and other anions play important roles in facilitating the binding of iron or manganese to proteins. For example, transferrins, a family of iron transport proteins, require bicarbonate or phosphate as a synergistic anion for iron binding.[13,14] Zwitterions also influence the assembly and catalytic properties of the tetranuclear manganese complex of photosystem II.[15,16] Upon the basis of the involvement of anions in metal binding in other proteins, the influence of anions on the Mn cofactor of the modified reaction centers was characterized and found to alter both the Mn binding affinity and electronic structure.[17] Since bicarbonate influences the Mn binding, it should also affect the energetics associated with the Mn cofactor.

The energetics of Mn oxidation were characterized using 10 mutants with the same three mutations that create the Mn binding site but different mutations near P that alter the $E_m(P/P^+)$ potential. The $E_m(P/P^+)$ potentials were electrochemically measured for each of the mutants and compared to the potentials found for mutants with the corresponding alterations near P but without the Mn binding site. By monitoring the extent of light-induced P^+ in each mutant using steady-state optical spectroscopy, the $E_m(Mn^{2+}/Mn^{3+})$ potentials in the absence and presence of bicarbonate were estimated. The different $E_m(Mn^{2+}/Mn^{3+})$ and $E_m(P/P^+)$ potentials result in a range of driving forces for Mn oxidation and charge recombination for the mutants. These electron transfer rates were measured using transient optical spectroscopy and related to the corresponding free energy differences using the Marcus equation.[18]

METHODS

Construction of Mutants, Protein Isolation, and Sample Preparation. The construction of the mutants was performed by

combining site-directed mutagenesis and manipulation of restriction fragments as previously described,[7,19] with the altered genes expressed in the *R. sphaeroides* deletion strain ΔLM1.1.[20] Cells were grown semiaerobically and the reaction centers were prepared as described earlier.[9,10] For spectroscopic measurements, after solubilization, the reaction centers were purified using DEAE Sephacryl ion exchange chromatography equilibrated with 0.05% Triton X-100 instead of 0.1% lauryl dimethylamine oxide. After the chromatography, the reaction centers were dialyzed against 15 mM Tris-HCl pH 8 and 0.05% Triton X-100 to remove EDTA.

P/P^+ Oxidation−Reduction Titrations. The $E_m(P/P^+)$ potentials were determined from electrochemical titrations of reaction centers using a system and analysis described previously.[7] Each titration was performed in both the oxidative and reductive direction to ensure reversibility. The reaction centers were prepared in 20 mM Tris-HCl pH 8, 0.1% Triton X-100, and 60 mM KCl (Aldrich-Sigma Chem. Co.). The mediators were 10 mM potassium hexacyano ferrate(III) (Aldrich-Sigma Chem. Co.), 0.15 mM potassium tetracyanomono(1,10-phenanthroline)ferrate (II) tetrahydrate, and 0.4 mM dicyanobis(1,10-phenanthroline)iron(II) dihydrate, of which the latter two were synthesized according to Schilt.[21] At any given ambient potential, the amount of P^+ present was determined by measurement of the amplitude of the P absorption band, which is at 865 nm in wild type and the mutants. The relative amount of P^+, $F(P^+)$, for each potential, E, was fitted using the Nernst equation:

$$F(P) = \left(1 + e^{-(E - E_m(P/P^+))\cdot(nF/RT)}\right)^{-1} \quad (1)$$

where F is Faraday's constant, n is the number of electrons, and $(nF/RT)^{-1}$ has a value of 0.03894 mV^{-1} at 298 K when n equals 1.

Measurement of Transient and Steady-State Absorption Changes. A Cary 5 spectrophotometer (Varian) was used to measure the steady-state optical absorbance changes induced by continuous illumination. The light excitation was achieved using an Oriel tungsten lamp with an 860 nm interference filter. The binding of Mn^{2+} was characterized by measurement of the fraction of P^+ in reaction centers in the presence of 0 to 1 mM $MnCl_2$. For each $MnCl_2$ concentration, the fraction of P^+ was measured from light-induced changes in the absorption spectrum from 700 to 1000 nm. For these measurements, the reaction centers were in 15 mM 2-[*n*-cyclohexylamino]ethane sulfonic acid pH 9 and 0.05% Triton X-100 with 100 μM terbutryne present to block electron transfer from Q_A to the secondary quinone.

The kinetics of the Mn^{2+} oxidation in the millisecond time scale were measured with a single beam spectrometer of local design.[22] A ND:YAG (Continuum) laser with a 5 ns laser pulse excited the reaction centers at 532 nm, and the transient change in absorption at 865 nm was monitored to determine the amount of P^+. The transient optical measurements were performed with 100 μM terbutryne to block electron transfer between the primary and secondary quinones. The recoveries were fit to one or two exponentials using a nonlinear least-squares method in order to determine the rate constants for charge recombination and the Mn^{2+} oxidation.

RESULTS

P/P^+ Oxidation−Reduction Midpoint Potential. To determine the $E_m(P/P^+)$ potentials, electrochemical measurements were performed on the mutants containing the Mn binding site changes, namely, Met M168 to Glu, Gly M288 to Asp, and Arg M164 to Tyr, as well as alteration of amino acid residues near P. The measured midpoint potentials for the mutants ranged from 480 mV to greater than 800 mV compared to 505 mV measured for wild type (Figure 2). In general, alteration of single amino acid residues near P resulted in an $E_m(P/P^+)$ increase of 35 to 100 mV compared to wild type, double mutations near P increased the midpoint potential by 120 to 180 mV, and a combination of three mutations near P raised the midpoint potential by 255 mV (Table 1). For the M2-9 mutant, only a limit of at least 800 mV could be established, as the measurements could not be reliably performed above that ambient potential. The mutant containing only the three changes associated with the Mn binding site and no alterations of the amino acid residues near P was found to have a decreased $E_m(P/P^+)$ potential of 480 mV, which is 25 mV less than wild type.

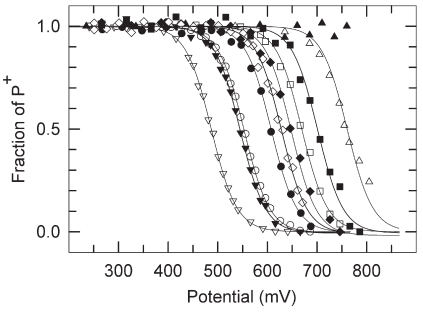

Figure 2. Electrochemical oxidation/reduction titrations of reaction centers. The fraction of P^+ was determined by monitoring the optical absorption at 865 nm for different ambient potentials. Shown are the data for the M2-1 (open down triangles), M2-2 (closed down triangles), M2-3 (open circles), M2-4 (closed circles), M2-5 (open diamonds), M2-6 (closed diamonds), M2-7 (open squares), M2-8 (closed squares), M2 (open up triangles), and M2-9 (closed up triangles) mutants. Titrations were performed in both oxidative and reductive directions to ensure reversibility. The lines represent fits of the data to the Nernst equation (eq 1). The $E_m(P/P^+)$ potentials for each mutant are summarized in Table 1. The individual titrations are shown separately in Figure 1 of the Supporting Information with the oxidative and reductive data identified.

Each titration was performed in both an oxidative and a reductive direction (Supplemental Figures S1−S10, Supporting Information), with the oxidative and reductive titrations being equivalent within the error of the measurements. For the mutants with the higher $E_m(P/P^+)$ potentials, full titrations could not be performed as poising the ambient potential above 800 mV resulted in a noticeable loss of the integrity of the sample. Therefore, for these mutants titrations were performed only to a maximum ambient potential of 800 mV. For each titration, the error of the fit was dependent primarily upon the completeness of the titration. Typically, the fits of the titrations using eq 1 had a least-squares error of 1−2 mV, while the error found for mutants with higher $E_m(P/P^+)$ potentials was 4−6 mV. As examples, fits of individual titrations of the M2-2, M2-6, and M2 mutants yielded least-squares errors of 1.3, 2.3, and 0.63, R factors of 0.999, 0.998, and 0.989, and residuals of 0.0003, 0.0005, and 0.0021, respectively. Despite a few titrations having some scatter of individual data points, the fits are highly constrained and the error of the one free parameter, namely, the $E_m(P/P^+)$ potential, is low. More accurate estimates for the errors associated with the

Table 1. P/P^+ Midpoint Potentials of Manganese-Binding Mutants

strain	redox mutations[a]	$E_m(P/P^+)$ (mV)[b]
M2-1	none	480
M2-2	Leu M160 to His	540
M2-3	Leu L131 to His	555
M2-4	Phe M197 to His	605
M2-5	Leu L131 to His and Leu M160 to His	625
M2-6	Phe M197 to His and Tyr M210 to Trp	650
M2-7	Leu M160 to His and Phe M197 to His	670
M2-8	Leu L131 to His and Phe M197 to His	690
M2	Leu L131 to His, Leu M160 to His, and Phe M197 to His	760
M2-9	Leu L131 to His, Leu M160 to His, Phe M197 to His, and Tyr M210 to Trp	>800

[a] In addition to the listed alterations, all mutants contain three substitutions designed to provide a Mn binding site: Arg M164 to Tyr, Met M168 to Glu, and Gly M288 to Asp. [b] The estimated error is ±5 mV for the mutants, except for M2 that had error of ±10 mV due to its higher $E_m(P/P^+)$ potential, and the M2-9 mutant for which only a lower limit could be established.

$E_m(P/P^+)$ potentials were determined from standard deviations of measurements that were performed two to six times each for each mutant. These standard deviations for the $E_m(P/P^+)$ potentials of the mutants ranged from 1.0 to 6.4 mV, with the standard deviations being generally more accurate for mutants with complete titrations than those with incomplete titrations, as was found for the standard errors associated with the individual titrations. For example, standard deviations of 1.3, 3.8, and 4.0 mV were obtained for the M2-2, M2-6, and M2 mutants, respectively. Upon the basis of these measurements, the estimated errors of the $E_m(P/P^+)$ potentials are ±5 mV for most mutants and ±10 mV for mutants with $E_m(P/P^+)$ potentials above 700 mV.

A second possible independent parameter in the Nernst Equation (eq 1) is n, representing the number of electrons transferred during the reduction/oxidation titration. For the fits described above, n was set equal to a value of 1. When n was treated as a free parameter, the least-squares fits of the different titrations yielded values ranging from 0.9 to 1.2, with fits of the full titrations yielding values of 1.0 ± 0.1. Within the error of the measurements, the $E_m(P/P^+)$ potentials obtained with n allowed to be a free parameter are the same as found with the constraint that n equals 1. Although noninteger values are allowed mathematically, the physically reasonable values must be integer, representing in this case the possible oxidation states of P. The different electronic states of P have been well characterized using a variety of spectroscopic techniques.[5] These studies have established the formation of the singly oxidized (cation radical) $P^{+\bullet}$ state due to light exposure or an increase in the ambient potential by chemical or electrochemical means. Therefore, the values reported for the $E_m(P/P^+)$ potentials are those determined with n fixed at a value of 1.

The $E_m(P/P^+)$ potentials of the mutants are expected to be approximately independent of pH as the $E_m(P/P^+)$ potential of wild type decreases by ~10 mV as the pH increases from 8.0 to 9.5.[23−25] To check that the alterations near P do not alter this pH dependence, the $E_m(P/P^+)$ potentials were measured at pH 9.5 for the mutants with single changes, namely, Leu to His at L131, Leu to His and M160, and Phe to His at M197. In all cases, the potential decreased by the same amount as wild type within the error of the measurements (data not shown) as is also true for mutations of Tyr M210 based upon extensive investigations.[11,26−29] To investigate the impact of the Mn binding site on the pH dependence, the $E_m(P/P^+)$ potential was measured at pH 9 for the M2-1 mutant, which has the Mn binding site but no alterations of residues near P compared to wild type. At pH 9, the potential was found to be 7 ± 5 mV lower than measured at pH 8, showing the same pH dependence as found for wild type. This pH dependence of the $E_m(P/P^+)$ potential is supported by proton release measurements of the M2 and other Mn binding mutants.[10] The Mn binding site has several ionizable amino acid residues (Figure 1). The binding of Mn results in a large proton release, approximately 1.4 protons per reaction center, and a pronounced pH dependence for Mn binding. However, only a small proton release is found upon Mn^{2+} oxidation, which is comparable to the proton release found in reaction centers without the Mn binding site.[10] The comparable proton release for the Mn binding mutant and wild type is consistent with a weak dependence of the $E_m(P/P^+)$ potential upon the pH value for all of the Mn binding mutants.

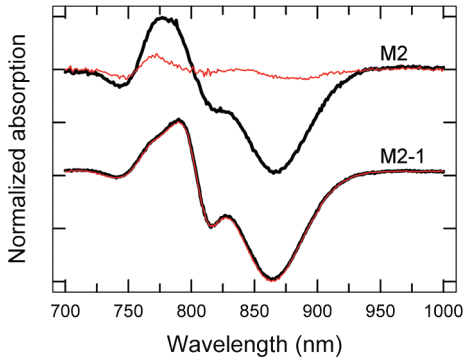

Figure 3. Effect of Mn on light-minus-dark optical spectra of the M2 and M2-1 mutants. For both the M2 and M2-1 mutants, in the absence of Mn, the steady-state light-minus-dark optical spectra show peaks characteristic of the $P^+Q_A^-$ charge-separated state, namely, an absorption decrease at 865 nm, and electrochromic shifts at 765 and 800 nm (black traces). In the presence of 10 μM Mn, the features associated with P^+ are not present although the features associated with Q_A^- remain for the M2 mutant (top red), while the M2-1 spectrum is essentially unchanged (bottom red).

Optical Spectra and Mn Binding. Each of the mutants exhibited an optical absorption spectrum characteristic of reaction centers, with near-infrared bands at 760, 800, and 865 nm, due to the bacteriopheophytins, monomeric bacteriochlorophylls, and P, respectively (data not shown). In the presence of light, the steady-state spectrum showed features that are characteristic of the formation of the charge-separated state $P^+Q_A^-$, including an absorption decrease near 865 nm due to P^+ and electrochromic shifts in the 770−800 nm region due to Q_A^- and P^+ (Figure 3). For all of the mutants and wild type, the spectra recovered fully after switching off the light. In the presence of Mn^{2+}, the light-minus-dark spectra changed to different degrees in the various mutants. For the M2 mutant, the spectrum showed

the features associated with Q_A^- but the extent of P^+ as determined from the absorption decrease at 865 nm was dependent upon the concentration of Mn^{2+}, with no P^+ evident at high concentrations of Mn^{2+}. The addition of Mn^{2+} led to a partial loss of the P^+ feature but a contribution from P^+ to the spectrum was always evident even at high Mn^{2+} concentrations for several mutants. For the M2-1 mutant, there were no changes when Mn^{2+} was present at any concentration.

The Mn binding measurements were performed at pH 9.0 as the dissociation constant sharply increases with decreasing pH below pH 8.5 due to the involvement of protonatable residues in the metal binding.[10,17] A small increase in the apparent dissociation constant was observed above pH 9, presumably due to the formation of insoluble manganese hydroxide and manganese carbonate compounds, which would act as a sink for the added manganese and lower the apparent activity. The effect became noticeable above pH 9.4, setting this pH value as the upper limit for the measurements.

This dependence of the spectral features on the Mn^{2+} concentration can be fitted assuming that the Mn-ion binds to the reaction center and serves as a secondary electron donor.[9] The dissociation constant of manganese binding to the reaction center, K_D, is related to the concentration of added Mn^{2+}, [Mn], and total concentration of reaction centers, [RC]:[9,30]

$$R_M = \frac{([Mn] + [RC] + K_D) - \sqrt{([Mn] + [RC] + K_D)^2 - 4[RC][Mn]}}{2[RC]} \quad (2)$$

where the fraction of reaction centers with bound metal, R_M, was found by monitoring the bleaching of the P band at 865 nm. Assuming the complete oxidation of Mn^{2+} bound to reaction centers, the fraction of reaction centers without bound metal ion is given by the ratio of the absorption change at 865 nm for reaction centers with manganese, ΔA_M^{865}, and in the absence of manganese, ΔA_0^{865}:

$$\frac{\Delta A_M^{865}}{\Delta A_0^{865}} = 1 - R_M \quad (3)$$

For each of the mutants, Mn^{2+} titrations yielded the same K_D of 1 μM for Mn^{2+} binding at pH 9. The consistency of the Mn^{2+} binding for all of the mutants shows that the Mn^{2+} binds at the designed metal binding site with the same binding affinity. Although the mutants have the same binding affinities for Mn, the effectiveness of Mn^{2+} at high concentrations in reducing P^+ was different for each mutant. The dependence of the effectiveness of Mn^{2+} as a secondary electron donor to P^+ can be modeled as being due to the difference between $E_m(P/P^+)$ and $E_m(Mn^{2+}/Mn^{3+})$. Light excitation leads to the formation of the charge-separated state $P^+Q_A^-$ when transfer between the two quinones is blocked by the presence of an inhibitor such as terbutryne. When Mn^{2+} is bound, a subsequent electron transfer takes place from the metal to reduce P^+, which competes with charge recombination:

$$Mn^{2+}\ PQ_A \xrightarrow{h\nu} Mn^{2+}\ P^*Q \rightarrow Mn^{2+}\ P^+Q_A^- \overset{\Delta G^0}{\Leftrightarrow} Mn^{3+}\ PQ_A^- \quad (4)$$

The amount of Mn^{3+} produced is dependent upon the free energy difference ΔG°. Since the last step in eq 4 is a simple one electron redox reaction, ΔG° can be expressed in terms of the difference in the midpoint potential for Mn, $E_m(Mn^{2+}/Mn^{3+})$ and the midpoint potential for P, $E_m(P/P^+)$:

$$\Delta G^\circ = nF[E_m(Mn^{2+}/Mn^{3+}) - E_m(P/P^+)] \quad (5)$$

where F is Faraday's constant and n, the number of electrons, is equal to 1. In order to fully oxidize the bound Mn^{2+}, the value of ΔG° must be large corresponding to $E_m(P/P^+)$ being well above the value of $E_m(Mn^{2+}/Mn^{3+})$, and no oxidation will be observed when ΔG° is positive due to $E_m(P/P^+)$ being smaller than $E_m(Mn^{2+}/Mn^{3+})$.

Thus, the amount of P^+ at high Mn^{2+} concentrations, $A(P^+)$, is obtained by the relative values of these two midpoint potentials as given by a modified form of the Nernst equation:

$$A(P^+) = \left(1 + e^{-((E_m(Mn^{2+}/Mn^{3+}) - E_m(P/P^+))/(nF/RT)}\right)^{-1} \quad (6)$$

By determining $A(P^+)$ from the Mn^{2+} titrations and the $E_m(P/P^+)$ potential through the electrochemical titrations, the value of $E_m(Mn^{2+}/Mn^{3+})$ can be directly accessed.

Using eq 6, the $E_m(Mn^{2+}/Mn^{3+})$ potential at pH 9 was determined to be 625 mV (Figure 4). Although there is some scatter to the data points relative to the fit, the $E_m(Mn^{2+}/Mn^{3+})$ potential is the only free parameter and the least-squares error is $\pm$5.5 mV, with an R factor of 0.952 and a residual of 0.008. When the number of electrons is fixed at two, the fits are significantly worse than those obtained for the one electron value, showing that the metal undergoes only a one-electron oxidation step (fits not shown). Allowing n to be a free parameter in the fitting with the $E_m(Mn^{2+}/Mn^{3+})$ potential yields a value of 1.0 $\pm$ 0.2, consistent with a one electron oxidation of the metal from Mn^{2+} to Mn^{3+}.

To determine any influence that bicarbonate may have on the $E_m(Mn^{2+}/Mn^{3+})$ values, the $E_m(Mn^{2+}/Mn^{3+})$ potential was also determined in the presence of 15 mM bicarbonate. The value of $A(P^+)$ measured in the presence of bicarbonate was found to be smaller for each mutant compared to the value without bicarbonate. Following the analysis described above, the lower values of $A(P^+)$ for each mutant results in a smaller $E_m(Mn^{2+}/Mn^{3+})$ value of 535 $\pm$ 6 mV at pH 9, with an R value of 0.93566 and a residual of 0.0058 (Figure 4). The addition of bicarbonate does not change the $E_m(P/P^+)$ potential

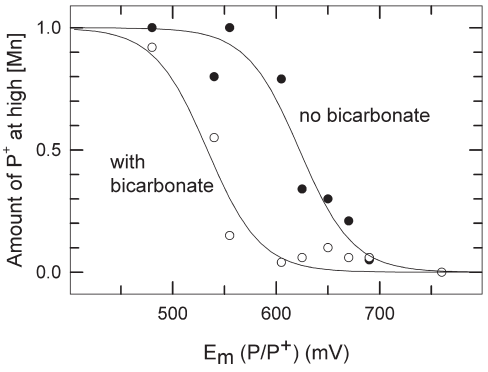

Figure 4. Determination of $E_m(Mn^{2+}/Mn^{3+})$ potentials. (A) The amount of P^+ at high Mn concentrations was determined for mutants with different $E_m(P/P^+)$ potentials. The resulting fits using eq 6 (solid lines) gave $E_m(Mn^{2+}/Mn^{3+})$ potentials of 535 mV with bicarbonate (open circles) and 625 mV without bicarbonate (closed circles).

dx.doi.org/10.1021/bi1017478 |*Biochemistry* 2011, 50, 3310–3320

of wild type within the error of the measurements (data not shown). Thus, the presence of the bicarbonate results in a 90 mV decrease in the $E_m(Mn^{2+}/Mn^{3+})$ value.

Electron Transfer Rates. In the absence of any metal, the light-induced charge-separated state $P^+Q_A^-$ recovered with rate constants ranging from 8.5 s^{-1} for the M2-1 mutant to 77 s^{-1} for the M2-9 mutant. The rate constants are correlated with the $E_m(P/P^+)$ potentials, as an increase in the midpoint potential corresponds to an increase in the free energy difference for charge recombination.[7] For each mutant, the $P^+Q_A^- \rightarrow PQ_A$ charge recombination rate was found to slightly increase as the pH increased from 7 to 9 as found in wild type and other mutants.[25]

For mutants with the low $E_m(P/P^+)$ potentials, the addition of Mn^{2+} did not measurably alter the kinetics of charge recombination. For these mutants, no or very small changes in the fraction of P^+ were observed in the steady-state measurements, which would correspond to only small changes in the contribution of the amplitude of the P^+ recovery compared to the contribution from charge recombination. Alternatively, no change in the observed rate of P^+ recovery would be observed if the rate of Mn^{2+} oxidation is comparable to or slower than the rate of $P^+Q_A^-$ charge recombination. However, for the mutants with $E_m(P/P^+)$ potentials significantly above the estimated $E_m(Mn^{2+}/Mn^{3+})$ potential, the overall recovery of P^+ was found to be faster in the presence of added Mn^{2+}. For these mutants with high $E_m(P/P^+)$ potentials, the recoveries were described with two exponential terms: a slower term that arises from $P^+Q_A^- \rightarrow PQ_A$ charge recombination, with the same rate constant as found in the absence of Mn^{2+}, and a faster term that is assigned to reduction of P^+ due to electron transfer from bound Mn^{2+}. Both of these terms were first-order as the fitted rate constants had no dependence on the Mn^{2+} concentration as has been previously reported for the M2 mutant.[9] The rate constant of Mn^{2+} oxidation showed a pronounced dependence on the $E_m(P/P^+)$ potential with faster rate constants being observed for mutants with higher potentials. In the absence of bicarbonate at pH 9.0, the rate constants of the component assigned to Mn oxidation were found to be 30, 40, 90, and 120 s^{-1} for the M2-7, M2-8, M2, and M2-9 mutants, respectively. In the presence of bicarbonate the rate increased for each mutant with measured rate constants of 65, 50, 100, and 165 s^{-1} for the M2-7, M2-8, M2, and M2-9 mutants, respectively.

DISCUSSION

The energetics of the bound Mn cofactor were probed through characterization of a series of mutants with both a Mn binding site and alterations near P (Figure 1). The optical spectra were essentially unchanged compared to wild type indicating that the arrangement of cofactors is the same. All of the mutants have the same Mn binding site and were found to bind Mn with a K_D of 1 μM. The measured $E_m(P/P^+)$ potentials of the mutants ranged from 480 to over 800 mV (Figure 2). This range of potentials provided the opportunity to relate the ability of the Mn cofactor to oxidize P^+ to the $E_m(P/P^+)$ potential while keeping the Mn binding site fixed. For mutants with low $E_m(P/P^+)$ potentials, the addition of Mn^{2+} had little or no effect on the light-induced P^+, but for mutants with high $E_m(P/P^+)$ potentials the amount of P^+ was greatly diminished when Mn^{2+} was added (Figure 3). The $E_m(Mn^{2+}/Mn^{3+})$ potentials determined using these spectral changes were 625 mV without bicarbonate and 535 mV with bicarbonate (Figure 4). For the mutants with high $E_m(P/P^+)$ potentials, the rate of recovery of the P^+ absorption band after illumination increased in the presence of Mn^{2+} due to electron transfer from the Mn^{2+}, allowing the determination of the rate constants of Mn^{2+} oxidation. Below, the energetics associated with the oxidation of the bound Mn^{2+} are discussed, including the relationship between the free energy differences and rates of charge recombination and Mn oxidation.

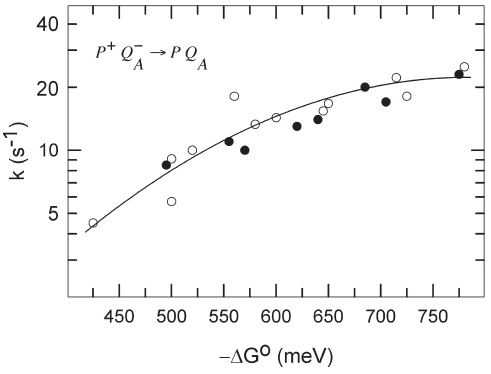

Figure 5. Marcus relationship for charge recombination. The dependence of the rate constant of $P^+Q_A^-$ charge recombination on the free energy difference for mutants containing the Mn binding site (closed circles) and without the Mn binding site (open circles). The line is a best fit of the data obtained from mutants without the Mn binding site using a Marcus relationship (eq 7) with a k_{max} and λ equal to 22.5 s^{-1} and 820 meV respectively as reported previously.[7,26] The rate constants obtained from the mutants with the Mn binding site are plotted but were not used in the fit.

Oxidation/Reduction Midpoint Potentials of P. The $E_m(P/P^+)$ potentials were determined using an electrochemical cell (Figure 2) and found to range from 480 mV to 760 mV (Table 1). For the corresponding mutants without the alterations associated with the Mn^{2+} binding site, the midpoint potential ranges from 505 for wild type to 765 mV.[7,8] Comparison of the $E_m(P/P^+)$ potentials for mutants with and without the metal-ion binding site, but identical alterations of residues near P, shows the potentials are systematically lower by ~20 mV due to the presence of the Mn binding site. The Mn^{2+} binding site is 10 Å from P and the 20 mV lowering of the $E_m(P/P^+)$ potential is likely due to the introduction of residues forming the Mn binding site. Similar decreases have been observed after the introduction of amino acid residues with carboxylic side chains at comparable distances from P.[25] For the M2-9 mutant, only a limit of at least 800 mV was established due to a lack of stability of this highly oxidizing mutant. However, a $E_m(P/P^+)$ potential of ~805 mV is likely based upon the 44−45 mV increase observed both for the M210 mutation compared to wild type[11] and for the double mutant Phe M197 to His and Tyr M210 to Trp compared to the single mutant Phe M197 to His (Table 1). The consistency of the $E_m(P/P^+)$ potentials for mutants with and without the Mn^{2+} binding site shows that the properties of the reaction center are generally not affected by the addition of the Mn binding site.

Dependence of the Rate of Charge Recombination on the Free Energy Difference. For the mutants containing the changes near P without the alterations to incorporate the Mn^{2+} binding site, the rate constant of $P^+Q_A^- \rightarrow PQ_A$ charge recombination systematically increases with increasing $E_m(P/P^+)$ potential.[7,31] For wild type, $P^+Q_A^-$ charge recombination has a ΔG° of −520 meV[32] and the changes in the $E_m(P/P^+)$ potential relative to wild

type are assumed to cause corresponding changes in the value of $\Delta G°$ in the mutants. For the mutants without the Mn binding site, the dependence of this rate constant on the $E_m(P/P^+)$ potential has been previously fitted using a Marcus relationship yielding a reorganization energy of 820 meV [7,31] (Figure 5). The mutants with the Mn binding sites follow the same dependence of the rate constants of $P^+Q_A^- \rightarrow PQ_A$ charge recombination on the $E_m(P/P^+)$ potentials. The exceptions to this agreement are the M2-6 and M2-9 mutants that each contains the mutation of Tyr M210 to Trp, which has a much faster recombination rate due to alteration of the energetics of the BChl monomer and bacteriopheophytin.[11,33,34] These results suggest that the introduction of the Mn binding site has only minor effects on the cofactors and their electron transfer properties.

Dependence of the Rate of Mn Oxidation on the Free Energy Difference. The availability of mutants that bind Mn with different $E_m(P/P^+)$ potentials provides the opportunity to determine the Marcus relationship for the metal-ion oxidation. The free energy difference for Mn^{2+} oxidation is determined by the difference in the $E_m(P/P^+)$ and $E_m(Mn^{2+}/Mn^{3+})$ potentials (eq 5). At any given pH, since all of the mutants under study have the same Mn binding site, the $E_m(Mn^{2+}/Mn^{3+})$ values are assumed to be the same with only the $E_m(P/P^+)$ potentials changing due to the mutations. Thus, each mutant has a different $\Delta G°$ and correspondingly should have a different rate constant, k, according to the Marcus relationship:

$$k = k_{max} e^{-(\Delta G^0 + \lambda)^2/(4\lambda k_B T)} \quad (7)$$

where λ is the reorganization energy, k_B is the Boltzmann constant, T is the temperature, and k_{max} is the maximum possible rate constant. The rate constant of Mn oxidation could only be determined from the $P^+Q_A^-$ recovery from mutants with high $E_m(P/P^+)$ potentials when the rate of Mn oxidation was measurably faster than the rate of $P^+Q_A^- \rightarrow PQ_A$ charge recombination.

For the mutants with high $E_m(P/P^+)$ potentials, namely, M2-7, M2-8, M2, and M2-9, the rate constants were measured in the absence and presence of bicarbonate. The rate constants systematically increase as $\Delta G°$ increases from −45 meV to −180 meV, assuming that the $E_m(P/P^+)$ potential of the M2-9 mutant is 805 mV as discussed above. The increase in the rate constants for each mutant in the presence of bicarbonate can be attributed as primarily arising from the lower $E_m(Mn^{2+}/Mn^{3+})$ potentials that result in higher $\Delta G°$ values ranging from −135 to −270 meV, assuming that bicarbonate does not alter other electron transfer characteristics.

A fit of the rates measured both in the absence and presence of bicarbonate yields a k_{max} of 170 s^{-1} and a reorganization energy of 290 meV (Figure 6). Because of the limited number of measurements, a unique fit could not be unambiguously determined. In particular, since the rate increases with increasing $\Delta G°$ throughout the entire range of the data, the value of 290 meV represents only a lower limit for the reorganization energy. For the separation distance of ∼10 Å between the bound Mn and P cofactors,[9] a k_{max} of 10^8 to 10^9 s^{-1} is predicted based upon electron transfer rates between cofactors with a similar separation distance in proteins.[35] For example, cytochrome c_2 bound to the reaction center has a similar distance of ∼10 Å to P but a much faster observed rate of 10^6 s^{-1} and an estimated k_{max} of 10^7 s^{-1}.[36] The slow rate of 170 s^{-1} may reflect the involvement of an unresolved rate-limiting step. For the M2 mutant, Fe^{2+} can also be bound to the metal binding site and is redox active, reducing P^+ with a rate constant of 175 s^{-1}.[37] Since the oxidation rate constants for both metals are comparable, the slowness of the reaction compared to the predicted rate is not due to specific characteristics of either metal. The relatively slow rate could reflect the electron transfer being coupled to a rate-limiting proton transfer process that is required to stabilize the change of charge of the Mn cofactor; however, the proton release upon metal oxidation is small.[10] More likely, the observed rate may reflect a significant difference between the free energy difference and reorganization energy. Specifically, a reorganization energy of 1500 meV rather than 300 meV would result in a k_{max} of ∼10^7 s^{-1} (eq 7) and suggest that the reorganization energy is significantly greater than the current estimate of at least 290 meV. This situation implies that the Mn binding site undergoes a large reorganization upon oxidation to Mn^{3+} that effectively limits the rate of electron transfer.

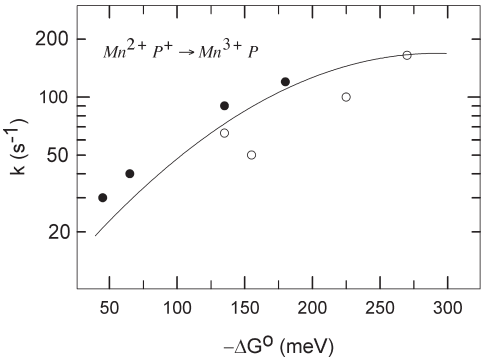

Figure 6. Marcus relationship for Mn oxidation. The dependence of the rate constant of Mn^{2+} oxidation on the free energy difference for mutants measured in the absence (closed circles) and presence of bicarbonate (open circles). The line is a best fit using a Marcus relationship (eq 7) with a k_{max} and λ equal to 152.5 s^{-1} and 290.5 meV, respectively. Because of the limited range of $\Delta G°$ for these rate constants, these parameters represent lower limits only.

Role of Bicarbonate. In solution, Mn^{2+} is very stable resulting in a high oxidation/reduction midpoint potential of the Mn^{2+}/Mn^{3+} couple of 1200−1500 mV for the aqua ions. By exchanging one or two coordinating water molecules with bicarbonate in the *hexa-aquo* complex, bicarbonate can bind directly to metal forming $Mn^{2+}(HCO_3)^+$ and $Mn^{2+}(HCO_3)_2$, respectively. The formation of such complexes are dependent on the bicarbonate concentration as the associations are weak and high bicarbonate concentrations are required.[38,39] The electrostatic stabilization by the coordination with bicarbonate significantly lowers the oxidation/reduction midpoint potential of the Mn^{2+}/Mn^{3+} couple in aqueous solutions by 300 and 600 mV compared to the *hexa-aquo* complex when one or two bicarbonates are bound, respectively.[38,39] For the M2 mutant, Mn binds with a dissociation constant of ∼1 μM at pH 9 both with and without bicarbonate.[17] As the pH is lowered without bicarbonate, the value of the dissociation constant sharply increases but is approximately independent of pH in the presence of bicarbonate. Bicarbonate probably coordinates the bound metal either as a bidentate or monodentate ligand and facilitates manganese binding by removing the requirement of proton release for metal binding to the M2 mutant.[17,37] Bicarbonate has also been shown to be necessary for the binding of Fe^{2+} to the M2 mutant.[37] In

the presence of bicarbonate, the $E_m(Mn^{2+}/Mn^{3+})$ potential of the bound Mn cofactor was found to decrease from 625 to 535 mV (Figure 4). These results are consistent with both bicarbonate and Mn^{2+} binding to the reaction center with the bicarbonate ligand lowering the $E_m(Mn^{2+}/Mn^{3+})$ potential due to the favorable electrostatic interactions.

Oxidation/Reduction Potentials of Mn Cofactors in Proteins. Proteins commonly make use of metal cofactors to drive redox reactions in biological organisms. For proteins containing Fe and Cu cofactors, there is an abundance of information concerning the electronic states of the metals, including the catalytically relevant oxidation/reduction midpoint potentials of the metals. In contrast, our knowledge of the electronic structures of Mn binding proteins is limited, partially because for many enzymes Mn^{2+} serves only a structural role and does not change oxidation state during the catalytic cycle. Below, we briefly compare our results for the $E_m(Mn^{2+}/Mn^{3+})$ potential with those known for other proteins with redox-active Mn cofactors.

The best-characterized redox-active Mn enzyme is Mn superoxide dismutase, which catalyzes the conversion of superoxide into molecular oxygen and hydrogen peroxide.[40,41] This enzyme contains a mononuclear Mn cofactor that cycles between the Mn^{2+} and Mn^{3+} states during catalysis with an oxidation/reduction midpoint potential ranging from 290 to 390 mV depending upon the source of the enzyme. In addition to studies of the wild-type superoxide dismutase, alteration of the residues near the metal binding site produced mutants with potentials ranging from 365 to 435 mV.[1] Closely related to these enzymes are the Fe superoxide dismutases that have a strong structural homology with the active site having the same metal coordination to three His, one Asp, and one solvent molecule.[42,43] The Fe superoxide dismutases have a lower oxidation/reduction midpoint potential of 220 mV in wild type, but when Mn is substituted into this metal binding site, the measured midpoint potential increases to over 960 mV, presumably due to changes in the hydrogen bonds involving the metal ligands.[44,45]

Mn peroxidase is a major component of the lignin-degrading metabolism of fungi and contains a Mn cofactor with one coordinating ligand provided by a propionate group from a nearby heme.[46] Mn^{2+} is converted into Mn^{3+} during catalysis and can be stabilized using chelators,[47] but determination of the oxidation/reduction midpoint potential of the Mn cofactor has been elusive.[48] The Mn cofactor of some other enzymes, such as Mn dioxygenase,[49,50] Mn lipoxygenase,[51] and oxalate decarboxylase,[52,53] can also be poised in different oxidation states that have been proposed to represent intermediate states of the Mn cofactor, but the midpoint potentials have not been determined. Several enzymes make use of a dinuclear Mn cofactor to facilitate catalysis.[54,55] For example, the enzyme Mn catalase facilitates the disproportionation of hydrogen peroxide into water and molecular oxygen. The Mn cofactor of Mn catalase has been characterized by a variety of spectroscopic techniques poised in the $(Mn^{2+})_2$, $(Mn^{2+}Mn^{3+})$, and $(Mn^{3+})_2$ states by the addition of substrates such as hydrogen peroxide or hydroxylamine; however the energetics of these states, including the oxidation/reduction midpoint potentials, have not been established.[54,56]

In contrast to the situation with Mn cofactors in proteins, a tremendous knowledge has been gained concerning the properties of Mn in synthesized compounds that are designed to mimic features of Mn cofactors in proteins.[55,57] For a wide array of compounds, the energetics of the electronic states, including the oxidation/reduction potentials of the associated Mn electronic states, have been determined. For example, synthetic mononuclear Mn^{2+} complexes can have potentials ranging from −1100 to +800 mV.[58−61] However, questions remain concerning the application of these results to Mn cofactors in proteins, for example, how the inhomogeneous protein environment can alter the energetics of Mn cofactors.

The measured $E_m(Mn^{2+}/Mn^{3+})$ potentials of 535 and 625 mV for the Mn binding reaction centers with and without bicarbonate fall within the range observed for superoxide dismutase as these values are higher than those measured for the wild type Mn superoxide dismutase but lower than the potential of Mn substituted into Fe-superoxide dismutase. The sensitivity to bicarbonate shows that changes in the Mn binding site can have large effects on the $E_m(Mn^{2+}/Mn^{3+})$ potential, consistent with the effect of ligands on the potentials observed for synthetic clusters. The approach described in this paper provides an experimental means of addressing outstanding questions concerning the impact of the protein environment on the metal cofactor potentials by measuring the $E_m(Mn^{2+}/Mn^{3+})$ potential under different experimental conditions. In particular, mutagenesis of the amino acid residues forming the metal binding site can be used to assess the impact of different protein−metal interactions, such as changes of metal coordination and electrostatic interactions, on the tuning of metal potentials to optimize oxidation/reduction reactions.

Implications for the Water Oxidation Complex. The bacterial reaction center and photosystem II have similar core structures, with both complexes having the key cofactors involved in the electron transfer events being surrounded by two core subunits, namely, the L and M subunits for the bacterial reaction center and the D1 and D2 subunits in photosystem II.[5,62] This structural homology allowed the Mn cofactor of the M2 mutant to be designed at a position analogous to the Mn_4Ca cofactor of photosystem II.[6,9] In photosystem II, the electron transfer reactions are more complex than those found in bacterial reaction centers, as the oxidized primary electron donor of photosystem II, $P680^+$, is initially reduced by Y_Z in a proton-coupled reaction followed by oxidation of the Mn_4Ca cofactor. The energetics associated with these reactions cannot be directly measured as they lie near or above the oxidation/reduction midpoint potential of water. However, estimates have been made based upon consideration of the electron transfer rates of these cofactors, yielding values of 1100−1250 mV for the oxidation/reduction midpoint potential of $P680/P680^+$, 970−1050 mV for Y_Z/Y_Z^+, and 700 mV for the initial oxidation step of the Mn_4Ca cofactor, namely, the S_0/S_1 transition.[63,64] Despite the relatively small free energy difference of ∼100 meV for electron transfer from Y_Z to P^+, the electron transfer is thought to proceed with a rate constant of 10^7 to 10^8 s^{-1}.[64] The much faster rate of $P680^+$ reduction in photosystem II compared to P^+ reduction in the M2 mutant probably reflects a much smaller reorganization energy of ∼100 meV for photosystem II that matches the free energy difference, making the observed rate nearly equivalent to k_{max}. There are many structural differences between the Mn cofactors in the M2 mutant and photosystem II that could contribute to this difference in reorganization energy. In particular, the Mn_4Ca cluster in photosystem II is deeply buried,[62] which would tightly restrain the allowed positions of the surrounding protein, while the Mn cofactor of the M2 mutant is close to the surface of the protein[9] and open to rearrangements of the surrounding protein after metal oxidation.

The Mn_4Ca cofactor of photosystem II has been well characterized through a wide array of spectroscopic techniques, but the molecular mechanism of water oxidation remains unsettled.[58] One question that continues to be debated is the involvement of bicarbonate in the assembly and function of the Mn_4Ca cofactor.[15,16,64−66] Bicarbonate has been proposed to function in a variety of roles, such as an electron donor,[67] ligand for the Mn_4Ca cofactor,[68,69] and substrate for the water oxidation process.[64,70] A bicarbonate molecule has been inconsistently included in the three-dimensional structures of the binding site of the Mn_4Ca cofactor, which is currently limited in quality due to the limited resolution of the models and radiation damage during X-ray exposure.[71−73] Comparison of several properties of the S states in photosystem II samples with and without bicarbonate led to the conclusion that the redox potentials of the S states were unaffected by the presence of bicarbonate.[69] The Mn_4Ca cofactor assembles in an unusual self-assembly process driven by the absorption of light by P680.[62,74] Our results are consistent with the model that bicarbonate facilitates the photoassembly by stabilizing the formation of an intermediate state, namely, a mononuclear Mn^{3+} cofactor.[15]

In addition to providing a platform for understanding how proteins modulate the energetics of Mn cofactors, the ability of the modified reaction centers to bind metals has implications for the evolutionary development of photosynthetic systems. The initial photosynthetic organisms present on the early Earth probably performed simple anoxygenic photochemistry involving low energy reactions as found today in purple bacteria.[6,64,75−79] In order to perform water oxidation, the primitive photosystems would have needed to become strong oxidants, couple the electron transfer with proton transfer, and develop the Mn_4Ca cofactor.[6,78] During the evolutionary development of oxygenic photosynthesis, the primitive complex could have gained a metal-binding site with only a limited number of amino acid alterations as found in the M2 mutant. In order for the manganese to serve as an efficient secondary electron donor, it would have been necessary to match the oxidation/reduction midpoint potentials of the Mn cofactor and the primary electron donor. The results of this paper show that the midpoint potential of the Mn cofactor could have been initially tuned by use of nonprotein ligands such as bicarbonate until the binding site gained ligands from peripheral protein subunits of photosystem II, especially the CP43 subunit. In addition, the primitive highly oxidizing reaction centers may have had functional properties, such as the ability to use reactive oxygen species as secondary electron donors, until they gained the capacity for water oxidation with the advent of the manganese cluster; work is underway to examine the possibility of this function in the M2 mutant.

■ ASSOCIATED CONTENT

Supporting Information. Oxidation/reduction titrations of the mutants, which are shown collectively in Figure 2, are presented individually for each mutant with the oxidative and reductive data identified. This material is available free of charge via the Internet at http://pubs.acs.org.

■ AUTHOR INFORMATION

Corresponding Author

*Phone: 480-965-8241. Fax: 480-965-2747. E-mail: jallen@asu.edu.

Present Addresses

‡Department of Physics, Concordia University, Montreal, Quebec H4B 1R6, Canada.

Funding Sources

This work was supported by Grant No. MCB 0640002 from the NSF.

■ ACKNOWLEDGMENT

We thank Lisa Lauman for assistance with the growth of the bacterial cells, Gregory Uyeda and Wei-Jen Lee for assistance with the mutagenesis, and Wei-Jen Lee and Paul Oyala for assistance with the spectroscopic measurements.

■ ABBREVIATIONS USED

P, primary electron donor of bacterial reaction center; P680, primary electron donor of photosystem II; Q_A, primary quinone acceptor; $E_m(P/P^+)$ potential, oxidation/reduction midpoint potential of primary electron donor; $E_m(Mn^{2+}/Mn^{3+})$ potential, oxidation/reduction midpoint potential of bound Mn cofactor

■ REFERENCES

(1) Lévêque, V. J. P., Vance, C. K., Nick, H. S., and Silverman, D. N. (2001) Redox properties of human manganese superoxide dismutase and active-site mutants. *Biochemistry 40*, 10586–10591.

(2) Vass, I., and Styring, S. (1991) pH-Dependent charge equilibria between tyrosine-D and the S states in Photosystem II: estimation of relative midpoint redox potentials. *Biochemistry 30*, 830–839.

(3) Tommos, C., and Babcock, G. T. (2000) Proton and hydrogen currents in photosynthetic water oxidation. *Biochim. Biophys. Acta 1458*, 199–219.

(4) Rappaport, F., and Diner, B. A. (2008) Primary photochemistry and energetics leading to the oxidation of the $(Mn)_4Ca$ cluster and to the evolution of molecular oxygen in photosystem II. *Coord. Chem. Rev. 252*, 259–272.

(5) Hunter, C. N., Daldal, F., Thurnauer, M. C., Beatty, J. T., Eds. (2008) *The Purple Phototrophic Bacteria*, Springer Verlag, Dordrecht, The Netherlands.

(6) Allen, J. P., and Williams, J. C. (2010) The evolutionary pathway from anoxygenic to oxygenic photosynthesis examined by comparison of the properties of photosystem II and bacterial reaction centers. *Photosynth. Res. 107*, 59–69.

(7) Lin, X., Murchison, H. A., Nagarajan, V., Parson, W. W., Allen, J. P., and Williams, J. C. (1994) Specific alteration of the oxidation potential of the electron donor in reaction centers from *Rhodobacter sphaeroides*. *Proc. Natl. Acad. Sci. U.S.A. 91*, 10265–10269.

(8) Kálmán, L., LoBrutto, R., Allen, J. P., and Williams, J. C. (1999) Modified reaction centres oxidize tyrosine in reactions that mirror photosystem II. *Nature 402*, 696–699.

(9) Thielges, M., Uyeda, G., Cámara-Artigas, A., Kálmán, L., Williams, J. C., and Allen, J. P. (2005) Design of a redox-linked active metal site: manganese bound to bacterial reaction centers at a site resembling that of photosystem II. *Biochemistry 44*, 7389–7394.

(10) Kálmán, L., Thielges, M. C., Williams, J. C., and Allen, J. P. (2005) Proton release due to manganese binding and oxidation in modified bacterial reaction centers. *Biochemistry 44*, 13266–13273.

(11) Nagarajan, V., Parson, W. W., Davis, D., and Schenck, C. C. (1993) Kinetics and free energy gaps of electron-transfer reactions in *Rhodobacter sphaeroides* reaction centers. *Biochemistry 32*, 12324–12336.

(12) Williams, J. C. Allen, J. P. (2008) Directed modification of reaction centers from purple bacteria, in *The Purple Phototrophic Bacteria* (Hunter, C. N., Daldal, F., Thurnauer, M. C., Beatty, J. T., Eds.) pp 337−353, Springer-Verlag, Dordrecht, The Netherlands.

(13) Harris, W. R., Nesset-Tollefson, D., Stenback, J. Z., and Mohamed-Hani, N. (1990) Site selectivity of binding of inorganic anions to serum transferrin. *J. Inorg. Biochem. 38*, 175–183.

(14) Dhungana, S., Taboy, C. H., Anderson, D. S., Vaughan, K. G., Aisen, P., Mietzner, T. A., and Crumbliss, A. L. (2003) The influence of the synergistic anion on iron chelation by ferric binding protein, a bacterial transferrin. *Proc. Natl. Acad. Sci. U. S. A. 100*, 3659–3664.

(15) Dasgupta, J., Tyryshkin, A. M., Baranov, S. V., and Dismukes, G. C. (2010) Bicarbonate coordinates to Mn^{3+} during photo-assembly of the catalytic Mn_4Ca core of photosynthetic water oxidation: EPR characterization. *Appl. Magn. Reson. 37*, 137–150.

(16) Ulas, G., and Brudvig, G. W. (2010) Zwitterion modulation of O_2-evolving activity of cyanobacterial photosystem II. *Biochemistry 49*, 8220–8227.

(17) Tang, K., Williams, J. C., Allen, J. P., and Kálmán, L. (2009) Effect of anions on the binding and oxidation of divalent manganese and iron in modified bacterial reaction centers. *Biophys. J. 96*, 3295–3304.

(18) Marcus, R. A., and Sutin, N. (1985) Electron transfers in chemistry and biology. *Biochim. Biophys. Acta 811*, 265–322.

(19) Williams, J. C. Taguchi, A. K. W. (1995) Genetic manipulation of purple photosynthetic bacteria, in *Anoxygenic Photosynthetic Bacteria* (Blankenship, R. E., Madigan, M. T., Bauer, C. E., Eds.) pp 1029−1065, Kluwer Academic Publishers, Dordrecht, The Netherlands.

(20) Paddock, M. L., Rongey, S. H., Feher, G., and Okamura, M. Y. (1989) Pathway of proton-transfer in bacterial reaction centers: Replacement of glutamic acid 212 in the L-subunit by glutamine inhibits quinone (secondary acceptor) turnover. *Proc. Natl. Acad. Sci. U.S.A. 86*, 6602–6606.

(21) Schilt, A. A. (1960) Mixed ligand complexes of iron(II) and (III) with cyanide and aromatic di-imines. *J. Am. Chem. Soc. 82*, 3000–3005.

(22) Kleinherenbrink, F. A., Chiou, H. C., LoBrutto, R., and Blankenship, R. E. (1994) Spectroscopic evidence for the presence of an iron-sulfur center similar to FX of photosystem I in *Heliobacillus mobilis*. *Photosynth, Res. 41*, 115–123.

(23) Maroti, P., and Wraight, C. A. (1988) Flash-induced H^+ binding by bacterial photosynthetic reaction centers: Influences of the redox states of the acceptor quinones and primary donor. *Biochim. Biophys. Acta 934*, 329–347.

(24) Ivancich, A., Mattioli, T. A., Artz, K. A., Wang, S., Allen, J. P., and Williams, J. C. (1997) Influence of Asn/His L166 on the hydrogen-bonding pattern and redox potential of the primary donor of purple bacterial reaction centers. *Biochemistry 36*, 3027–3036.

(25) Williams, J. C., Haffa, A. L. M., McCulley, J. L., Woodbury, N. W., and Allen, J. P. (2001) Electrostatic interaction between charged amino acid residues and the bacteriochlorophyll dimer in reaction centers from *Rhodobacter sphaeroides*. *Biochemistry 40*, 15403–15407.

(26) Gunner, M. R., Nicholls, A., and Honig, B. (1996) Electrostatic potentials in *Rhodopseudomonas viridis* reaction centers: Implications for the driving force and directionality of electron transfer. *J. Phys. Chem. 100*, 4277–4291.

(27) Beekman, L. M. P., van Stokkum, I. H. M., Monshouwer, R., Rijnders, A. J., McGlynn, P., Visschers, R. W., Jones, M. R., and van Grondelle, R. (1996) Primary electron transfer in membrane-bound reaction centers with mutations at the M210 position. *J. Phys. Chem. 100*, 7256–7268.

(28) Alden, R. G., Parson, W. W., Chu, Z. T., and Warshel, A. (1996) Orientation of the OH dipole of tyrosine (M)210 and its effect on electrostatic energies in photosynthetic bacterial reaction centers. *J. Phys. Chem. 100*, 16761–16770.

(29) Zhou, H., and Boxer, S. G. (1998) Probing excited-state electron transfer by resonance Stark spectroscopy. 2. Theory and application. *J. Phys. Chem. 102*, 9148–9160.

(30) Gerencsér, L., and Maróti, P. (2001) Retardation of proton transfer caused by binding of the transition metal ion to the bacterial reaction center is due to pK_a shifts of key protonatable residues. *Biochemistry 40*, 1850–1860.

(31) Allen, J. P., Williams, J. C., Graige, M. S., Paddock, M. L., Labahn, A., Feher, G., and Okamura, M. Y. (1998) Free energy dependence of the direct charge recombination from the primary and secondary quinones in reaction centers from *Rhodobacter sphaeroides*. *Photosynth. Res. 55*, 227–233.

(32) Arata, H., and Parson, W. W. (1981) Delayed fluorescence from *Rhodopseudmonas sphaeroides* reaction centers: enthalpy and free energy changes accompanying electron transfer from P-870 to quinones. *Biochim. Biophys. Acta 638*, 201–209.

(33) Kirmaier, C., and Holten, D. (2009) Low-temperature studies of electron transfer to the M side of YFH reaction centers from *Rhodobacter capsulatus*. *J. Phys. Chem. B 113*, 1132–1142.

(34) Pawlowicz, N. P., van Stokkum, I. H. M., Breton, J., van Grondelle, R., and Jones, M. R. (2010) An investigation of slow charge separation in a tyrosine M210 to tryptophan mutant of the *Rhodobacter sphaeroides* reaction center by femtosecond mid-infrared spectroscopy. *Phys. Chem. Chem. Phys. 12*, 2693–2705.

(35) Moser, C. C., Keske, J. M., Warncke, K., Farid, R. S., and Dutton, P. L. (1992) Nature of biological electron transfer. *Nature 355*, 796–802.

(36) Lin, X., Williams, J. C., Allen, J. P., and Mathis, P. (1994) Relationship between rate and free energy difference for electron transfer from cytochrome c_2 to the reaction center in *Rhodobacter sphaeroides*. *Biochemistry 33*, 13517–13523.

(37) Kálmán, L., LoBrutto, R., Williams, J. C., and Allen, J. P. (2006) Iron as a bound secondary electron donor in modified bacterial reaction centers. *Biochemistry 45*, 13869–13874.

(38) Dismukes, G. C., Klimov, V. V., Baranov, S. V., Kozlov, Y. N., DasGupta, J., and Tyryshkin, A. (2001) The origin of atmospheric oxygen on Earth: The innovation of oxygenic photosynthesis. *Proc. Natl. Acad. Sci. U.S.A. 98*, 2170–2175.

(39) Ananyev, G. M., Zaltsman, L., Vasko, C., and Dismukes, G. C. (2001) The inorganic biochemistry of photosynthetic oxygen evolution/water oxidation. *Biochim. Biophys. Acta 1503*, 52–68.

(40) Miller, A.-F. (2001) Fe superoxide dismutases, in *Handbook of Metalloproteins* (Messerschmidt, A., Huber, R., Poulos, T., Wieghardt, K., Eds.) pp 668−682, John Wiley, New York.

(41) Miller, A.-F. (2004) Superoxide dismutases: active sites that save, but a protein that kills. *Curr. Opin. Chem. Biol. 8*, 162–168.

(42) Lah, M. S., Dixon, M. M., Pattridge, K. A., Stallings, W. C., Fee, J. A., and Ludwig, M. L. (1995) Structure−function in *Escherichia coli* iron superoxide dismutase: Comparisons with the manganese enzyme from *Thermus thermophilus*. *Biochemistry 34*, 1646–1660.

(43) Perry, J. J. P., Shin, D. S., Getzoff, E. D., and Tainer, J. A. (2010) The structural biochemistry of the superoxide dismutases. *Biochim. Biophys. Acta 1804*, 245–262.

(44) Yikilmaz, E., Rodgers, D. W., and Miller, A.-F. (2006) The crucial importance of chemistry in the structure-function link: Manipulating hydrogen bonding in iron-containing superoxide dismutase. *Biochemistry 45*, 1151–1161.

(45) Vance, C. K., and Miller, A.-F. (2001) Novel insights into the basis for *Escherichia coli* superoxide dismutase's metal-ion specificity from Mn-substituted FeSOD and its very high E_m. *Biochemistry 40*, 13079–13087.

(46) Gold, M. H., Youngs, H. L., Sollewijn Gelpke, M. D. (2000) Manganese peroxidase, in *Manganese and Its Role in Biological Systems* (Sigel, A. Sigel, H., Eds.) pp 559−586, Marcel Dekker Publishers, New York.

(47) Wariishi, H., Valli, K., and Gold, M. H. (1992) Manganese(II) oxidation by manganese peroxidase from the basidiomycete *Phanerochaete chrysosporium*. *J. Biol. Chem. 267*, 23688–23695.

(48) Petruccioli, M., Frasconi, M., Quaratino, D., Covino, S., Favero, G., Mazzei, F., Federici, F., and D'Annibale, A. (2009) Kinetic and redox properties of MnP II, a major manganese peroxidase isoenzyme from *Panus tigrinus* CBS 577.79. *J. Biol. Inorg. Chem. 14*, 1153–1163.

(49) Gunderson, W. A., Zatsman, A. I., Emerson, J. P., Farquhar, E. R., Que, L., Jr., Lipscomb, J. D., and Hendrich, M. P. (2008) Electron

paramagnetic resonance detection of intermediates in the enzymatic cycle of an extradiol oxygenase. *J. Am. Chem. Soc. 130*, 14465–14467.

(50) Emerson, J. P., Kovaleva, E. G., Farquhar, E. R., Lipscomb, J. D., and Que, L., Jr. (2008) Swapping metals in Fe- and Mn-dependent dioxygenases: Evidence for oxygen activation without a change in metal redox state. *Proc. Natl. Acad. Sci. U.S.A. 105*, 7347–7352.

(51) Su, C., Sahlin, M., and Oliw, E. H. (2000) Kinetics of manganese lipoxygenase with a catalytic mononuclear redox center. *J. Biol. Chem. 275*, 18830–18835.

(52) Chang, C. H., Svedruzic, D., Ozarowski, A., Walker, L., Yeagle, G., Britt, R. D., Angerhofer, A., and Richards, N. G. J. (2004) EPR spectroscopic characterization of the manganese center and a free radical in the oxalate decarboxylase reaction. *J. Biol. Chem. 279*, 52840–52849.

(53) Moomaw, E. W., Angerhofer, A., Moussatche, P., Ozarowski, A., Garcia-Rubio, I., and Richards, N. G. J. (2009) Metal dependence of oxalate decarboxylase activity. *Biochemistry 48*, 6116–6125.

(54) Dismukes, G. C. (1996) Manganese enzymes with binuclear active sites. *Chem. Rev. 96*, 2909–2926.

(55) Wu, A. J., Penner-Hahn, J. E., and Pecoraro, V. L. (2004) Structural, spectroscopic, and reactivity models for the manganese catalases. *Chem. Rev. 104*, 903–938.

(56) Yoder, D. W., Hwang, J., Penner-Hahn, J. E. (2000) Manganese peroxidase, in *Manganese and Its Role in Biological Systems* (Sigel, A. Sigel, H., Eds.) pp 527−557, Marcel Dekker Publishers, New York.

(57) Mukhopadhyay, S., Mandal, S. K., Bhaduri, S., and Armstrong, W. H. (2004) Manganese clusters with relevance to photosystem II. *Chem. Rev. 104*, 3981–4026.

(58) McEvoy, J. P., and Brudvig, G. W. (2006) Water-splitting chemistry of photosystem II. *Chem. Rev. 106*, 4455–4483.

(59) Gupta, R., and Borovik, A. S. (2003) Monomeric $Mn^{III/II}$ and $Fe^{III/II}$ complexes with terminal hydroxo and oxo ligands: Probing reactivity via O-H bond dissociation energies. *J. Am. Chem. Soc. 125*, 13234–13242.

(60) Scarpellini, M., Gatjens, J., Martin, O. J., Kampf, J. W., Sherman, S. E., and Pecoraro, V. L. (2008) Modeling the resting state of oxalate oxidase and oxalate decarboxylase enzymes. *Inorg. Chem. 47*, 3584–3593.

(61) Sjodin, M., Gatjens, J., Tabares, L. C., Thuery, P., Pecoraro, V. L., and Un, S. (2008) Tuning the redox properties of manganese(II) and its implications to the electrochemistry of manganese and iron superoxide dismutase. *Inorg. Chem. 47*, 2897–2908.

(62) Wydrzynski, T. Satoh, K., Eds. (2005) *Photosystem II: The Light-Driven Water: Plastoquinone Oxidoreductase*, Springer Publishers, Dordrecht, The Netherlands.

(63) Tommos, C., and Babcock, G. T. (2000) Proton and hydrogen currents in photosynthetic water oxidation. *Biochim. Biophys. Acta 1438*, 199–219.

(64) Dismukes, G. C., Klimov, V. V., Baranov, S. V., Kozlov, Y. N., DasGupta, J., and Tyryshkin, A. (2001) The origin of atmospheric oxygen on Earth: The innovation of oxygenic photosynthesis. *Proc. Natl. Acad. Sci. U.S.A. 98*, 2170–2175.

(65) Shevela, D., Klimov, V., and Messinger, J. (2007) Interactions of photosystem II with bicarbonate, formate, and acetate. *Photosynth. Res. 94*, 247–264.

(66) Ulas, G., Olack, G., and Brudvig, G. W. (2008) Evidence against bicarbonate bound in the O_2-evolving complex of photosystem II. *Biochemistry 47*, 3073–3075.

(67) Klimov, V. V., Allakhverdiev, S. I., Feyziev, Y. M., and Baranov, S. V. (1995) Bicarbonate requirement for the donor side of photosystem II. *FEBS Lett. 363*, 251–255.

(68) Klimov, V. V., Hulsebosch, R. J., Allakhverdiev, S. I., Wincencjusz, H., van Gorkom, H. J., and Hoff, A. J. (1997) Bicarbonate may be required for ligation of manganese in the oxygen-evolving complex of photosystem II. *Biochemistry 36*, 16277–16281.

(69) Shevela, D. N., Khorobrykh, A. A., and Klimov, V. V. (2006) Effect of bicarbonate on the water-oxidizing complex of photosystem II in the super-reduced S-states. *Biochim. Biophys. Acta 1757*, 253–261.

(70) Warburg, O. (1964) Introduction. *Annu. Rev. Biochem. 33*, 1–15.

(71) Ferreira, K. N., Iverson, T. M., Maghlaoui, K., Barber, J., and Iwata, S. (2004) Architecture of the photosynthetic oxygen-evolving center. *Science 303*, 1831–1838.

(72) Loll, B., Kern, J., Saenger, W., Zouni, A., and Biesiadka, J. (2005) Towards complete cofactor arrangement in the 3.0 Å resolution structure of photosystem II. *Nature 438*, 1040–1044.

(73) Yano, J., Kern, J., Sauer, K., Latimer, M. J., Pushkar, Y., Biesiadka, J., Loll, B., Saenger, W., Messinger, J., Zouni, A., and Yachandra, V. K. (2005) Where water is oxidized to dioxygen: Structure of the photosynthetic Mn_4Ca cluster. *Science 314*, 821–825.

(74) Ono, T. (2001) Metallo-radical hypothesis for photoassembly of $(Mn)_4$-cluster of photosynthetic oxygen evolving complex. *Biochim. Biophys. Acta 1503*, 40–51.

(75) Olson, J. M., and Pierson, B. K. (1987) Origin and evolution of photosynthetic reaction centers. *Orig. Life. Evol. Biosph. 17*, 419–430.

(76) Blankenship, R. E., and Hartman, H. (1998) The origin and evolution of oxygenic photosynthesis. *Trends Biochem. Sci. 23*, 94–97.

(77) Larkum, A. W. D. (2006) The evolution of chlorophylls and photosynthesis, in *Chlorophylls and Bacteriochlorophylls* (Grimm, B., Porra, R. J., Rudiger, W., Scheer, H., Eds.) pp 261−282, Springer-Verlag, Dordrecht, The Netherlands.

(78) Williamson, A., Conlan, B., Hillier, W., and Wydrzynski, T. (2010) The evolution of photosystem II: insights into the past and future. *Photosynth. Res. 107*, 71–86.

(79) Leslie, M. (2009) On the origin of photosynthesis. *Science 323*, 1286–1287.